A Reproducible Bioimpedance Transducer for Insulin Noninvasive Measurement

Pasquale Arpaia, *Senior Member, IEEE*, Francesca Mancino, and Nicola Moccaldi, *Member, IEEE*

***Abstract*— A bioimpedance transducer is proposed for noninvasive monitoring of insulin bioavailability after subcutaneous injection. The insulin bioavailability is assessed indirectly by measuring the local impedance variation due to the drug disappearance from the injection volume. The instrument allows to manage the extreme variability in insulin response by patients with diabetes due to skin conditions and/or alterations such as lipodystrophy. In this way, the transducer can also be considered as a key component for new generation of artificial pancreas. The instrument achieves the state-of-the-art accuracy and uncertainty. Intraindividual reproducibility also improved with respect to previous studies. Moreover, the feasibility of an absorption measurement is proven. After presenting the concept design and the prototype, the metrological characterization during: 1) laboratory (on passive electrical components); 2) in vitro (on eggplants); and 3) in vivo (on a human subject) experiments is reported. In laboratory tests, typical percentage deterministic errors of 1% on magnitude and phase were obtained. The mean 1-σ repeatability of 0.05% was obtained for both impedance magnitude and phase. The in vitro tests were aimed to improve the reproducibility by comparing the electrical behavior of insulin and vehicle in eggplants. During in vivo tests, a decrease in percentage 1-σ intraindividual reproducibility was reported with respect to the state-of-the-art (from more than 200% to 36%), as the impedance magnitude is concerned. In a clinical application framework, an accuracy of 9 μl was obtained by means of a second-order polynomial model. The uncertainty was 4.2 μl, well below the typical volume of one insulin unit (10.0 μl).**

***Index Terms*— Bioimpedance spectroscopy, diabetes, insulin bioavailability, metrological characterization, soft transducer.**

I. Introduction

THE number of people with type 1 diabetes in the world is about 10 million [1].

The pancreas regulates insulin production based on continuous monitoring of blood glucose levels. Insulin lets sugar (glucose) enter cells to produce energy. Type 1 diabetes is a chronic disease caused by an immune-associated or immune-mediated destruction of insulin-producing β cells of pancreas [2], [3]. Patients with Type 1 diabetes need a continuous lifelong exogenous insulin replacement. However, insulin administration without continuous glucose monitoring does not always ensure proper metabolic regulation leading to one or more disease-associated complications (e.g., hypoglycemia, neuropathy, retinopathy, and cardiovascular disease) [4]. Therefore, for patients with type 1 diabetes, monitoring of blood glucose concentration (BGC) and its regulation through daily insulin injections are the pillars of the treatment [5], [6]. In the past years, real-time continuous glucose monitoring systems replaced self-monitored blood glucose procedures. Recently, a new generation of sensors for noninvasive BGC monitoring is emerging. One of the main noninvasive approaches is the infrared-spectroscopy-based method. The mid-infrared (MIR) and near-infrared (NIR) spectroscopy are based on the absorption measurement of light in 2500–10 000-nm and 750–2500-nm region of the spectrum, respectively. In the MIR bandwidth, the peak glucose response is sharper than the NIR bandwidth [7]. Differently, NIRs appear very promising for noninvasive glucose measurement because of the deep penetration ability [8]. However, these methods have not yet reached an acceptable level of accuracy in clinical application [9]. Other noninvasive devices are the resonator-based biosensors. They quantitatively assess BGC levels by exploiting the level of electromagnetic coupling depending on glucose permittivity [10], [11]. These biosensors are low costs, high robust, and allow real-time BGC detection [12]. However, they are affected by poor sensitivity. Finally, 3-D-printed approaches are also gradually increasing. For example, the e-ring for nonenzymatic glucose monitoring in sweat shows high sensitivity and wearability. However, the development of these sensors requires complex and laborious procedures, which affects their still too high costs [13].

Nowadays, an emerging automated treatment to improve BGC regulation is the artificial pancreas (AP) [14]. The AP: 1) monitors BGC levels through a BGC transducer and 2) controls an insulin pump to deliver the required amount of insulin (closed loop). However, this closed loop does not work properly during meals because of the sudden and large changes in glucose levels produced by food ingestion. In fact, glucose checking takes place in the interstitial fluid, and therefore, it is accompanied by a physiological time delay from plasma concentrations [15]. Therefore, before meals, the loop is opened and the patient injects an appropriate amount of insulin (bolus). The bolus is calculated by dedicated algorithms based on several inputs, including insulin sensitivity factor (ISF) and insulin duration of action (IDA). To date, the levels of ISF and IDA are fixed during the initial calibration of the algorithm used to compute the insulin dosages. However, the factors widely differ between individuals and impact the insulin uptake kinetics (bioavailability). For example, a skin alteration such as lipodystrophy can significantly alter the estimation of ISF [16]. Moreover, in diabetic therapies, insulin

Manuscript received 28 November 2022; revised 21 February 2023; accepted 14 March 2023. Date of publication 3 April 2023; date of current version 13 April 2023. This work was supported by the IEEE Instrumentation and Measurement Graduate Fellowship Award 2021 won by Francesca Mancino. The Associate Editor coordinating the review process was Dr. Jagadeesh Varadarajan Kumar. *(Corresponding author: Pasquale Arpaia.)*

The authors are with the Department of Electrical Engineering and Information Technology (DIETI), University of Naples Federico II Naples, 80131 Naples, Italy (e-mail: pasquale.arpaia@cern.ch).

Digital Object Identifier 10.1109/TIM.2023.3264037

doses and injection intervals are empirically estimated. Consequently, it is complex to predict glycemic fluctuation because of individual differences in insulin bioavailability. Currently, there is a lack of noninvasive methods to real-time assess the absorption of insulin from the site of administration.

To date, drug bioavailability can be assessed in vitro (Franz diffusion cell [17]), ex vivo (e.g., tape stripping technique [18]), or in vivo (e.g., skin biopsy [19], suction blister [20], micro dialysis [21], and confocal Raman spectroscopy [22]). Excluding the in vitro methods characterized by high accuracy but low usability for routine applications, each of the other methods has clinical limitations. Skin biopsies and suction blisters allow precise measurements, but have a high invasiveness and latency. Tape stripping and microdialysis are less invasive, but hard to standardize. Confocal Raman spectroscopy requires very expensive equipment and only allows direct analysis of the most superficial skin layers.

As far as insulin bioavailability assessment is concerned, the previously mentioned glucose sensors represent a noninvasive and low-cost solution. However, their latency prevents real-time applications.

For several years now, bioimpedance has emerged as a method to simultaneously pursue noninvasiveness, low-cost, and real-time. The bioimpedance spectroscopy is extensively used in several biomedical applications [23], [24], [25], [26], [27].

In [28] and [29], an impedance spectroscopy-based method was proposed to measure the amount of drug under the skin. In [30], the method was used for assessing insulin bioavailability after subcutaneous injections. The method is based on a personalized model linking impedance magnitude variation to drug amount variation, identified during insulin injection once the dosage is known (*appearance model*). The *disappearance model* (i.e., the inverse of the appearance model) allows to use impedance magnitude variation to estimate the amount of insulin that leaves the injection site and thus is absorbed. However, the feasibility study of the method highlighted huge variability among the personalized models. Moreover, the method did not manage the impact of mechanical noise sources (e.g., the pressure exerted during the injection phase, breathing) on the measurements [31], [32].

Subsequent tests [33] showed the significant impact of mechanical noise sources (e.g., the pressure exerted during injection and breathing) on method reproducibility. It is worth noting that this method was only based on impedance magnitude measurements and the impedance phase was not exploited.

In this article, a transducer for noninvasive insulin measurement is presented and metrologically characterized. The research goals were to handle the mechanical sources of noise and to achieve the requirements for clinical applications, i.e., accuracy and uncertainty below the typical volume of a unit of insulin (i.e., 10 μl).

In particular, Section II reports the bioimpedance transducer design; Section III describes the bioimpedance transducer realization; Sections IV and V report the metrological characterization of the bioimpedance transducer in eggplants and humans, respectively; finally, the feasibility of an absorption measurement is presented in Section VI.

II. Design

A. Basic Ideas

From a conductometric point of view, a generic tissue can be approximated as an electrolyte solution containing a large number of cells [34], [35]. The solute amount in a solution can be assessed by conductivity measurements. In detail, the addition of a conductive solute into a solution produces a variation in the resistance. Likewise, an amount of drug injected into a biological tissue (characterizable by dielectric relaxation phenomena and ionic conductivity) can be assessed by impedance measurements [36]. Starting from these considerations, the concept design of the bioimpedance transducer was based on the following basic ideas.

1) The insulin bioavailability can be indirectly assessed by measuring the drug disappearance from the injection site.
2) The insulin disappearance can be noninvasively assessed by tissue impedance measurements. In fact, the injection of a drug into a tissue produces an impedance variation. The same variation, in the opposite direction, is caused by the disappearance of the drug during its absorption.
3) The percentage variation in impedance magnitude with respect to a *reference value* (acquired in the preinjection phase) is linked to the insulin amount by an almost linear relationship.
4) At each new insulin administration, a specific personalized relationship between insulin amount and impedance variation can be identified. In this way, intra- and interindividual reproducibility issues can be managed.
5) The effect of significant mechanical sources of uncertainty can be managed by waiting for the transient attenuation.
6) The *reference value* for the computation of impedance percentage variation is measured after needle introduction. In this way, the bias due to syringe's pressure on the tissue until needle extraction is taken into account.

B. Architecture

The architecture of the bioimpedance transducer is shown in Fig. 1.

Four electrodes are placed on the tissue under test centered on the insulin bolus point of injection. The impedance meter applies a sinusoidal current through the amperometric electrodes on tissue and acquires the correspondent voltage drop through the voltmeters' electrodes. The signal conditioning is accomplished through the analog front-end. The smart insulin pen administers the insulin bolus at n units for step. For each step of injection, the smart insulin pen communicates: 1) the start of injection to the mechanical transient attenuation checker and 2) the number of insulin units administrated to the personalized model identifier. The impedance meter acquires the impedance of the tissue under test and sends the values to

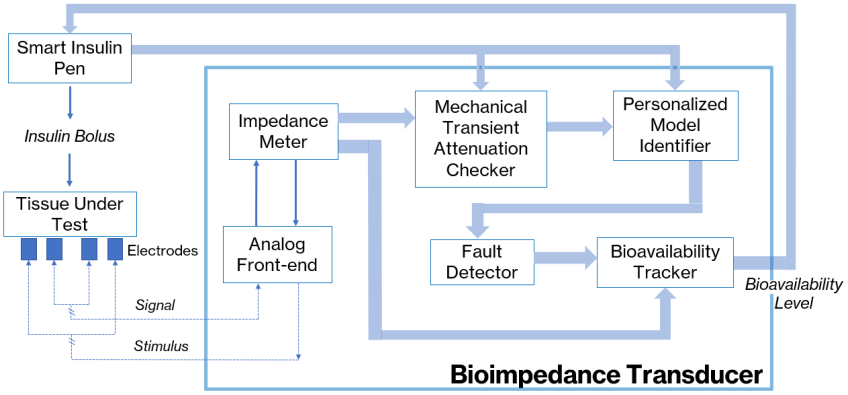

Fig. 1. Architecture of the bioimpedance transducer for noninvasive measurement of insulin.

the mechanical transient attenuation checker. The mechanical transient attenuation checker calculates the absolute value of the difference between the current and previous values. The mechanical transient attenuation checker sends the data to the personalized model identifier if the standard deviation of six consecutive differences, selected with a sliding time window of 1 s, remains in an experimentally defined range.

This range was defined basing on preliminary study on the impact of pressure on the impedance magnitude variation. A preliminary experimental campaign was conducted on 30 subjects to acquire typical impedance variation trend in case of resting state (absence of mechanical stresses and controlled breathing) at 10 kHz. For each measurement, the absolute value of the difference between the current and previous impedance magnitude values (*abs_im*) is computed and inserted in the resting state track (rs_i) for the ith subject. A sliding time window (win) of 1 s extracts six consecutive *abs_im* from the ith rs_i vector. The *win* slides one *abs_im* at a time. The standard deviation is calculated for each *win* (σ_win_i) of each rs_i and inserted in the standard deviation vector of all the subjects (subj_σ). The mean (all_μ) and standard deviation (all_σ) of the subj_σ are computed. The range for triggering the mechanical transient attenuation checker is the sum of all_μ and all_σ and was found equal to 0.05 Ω.

In this way, the mechanical transient attenuation checker waits for the suitable attenuation of the tissue mechanical phenomena. Then, the personalized model identifier approximates the relationship between 1) the insulin amount values received from the smart insulin pen and 2) the impedance values filtered from the mechanical transient attenuation checker. Subsequently, the fault detector checks the personalized model parameters experimentally identified during injections. If the parameters are within the uncertainty limits experimentally defined, the *Bioavailability Tracker* calculates the insulin disappeared (namely absorbed) from the volume of tissue under test.

The uncertainty limits are defined as the mean ± standard deviation of the generic model calculated during the in vivo experimental campaign.

C. Operation

The operating procedure of the bioimpedance transducer is described below.

1) *Electrodes Application:* FIAB 500 pregelled electrodes were used for the measurements.
2) *Waiting for the Instrumentation Warm-Up:* the measures started after the end of the warm-up time of the instrument (30 s). In this way, the signal oscillations remain below a fixed threshold.
3) *Reference Value Identification:* 10 s after needle introduction, the mean of the ten consecutive impedance values is calculated, and the successive impedance measurements are normalized to this value.
4) *Model Identification:* After each step of injection, the mean of ten consecutive impedance values is computed. Given the percentage impedance variations (PIVs) with respect to the reference value and the amount of drugs delivered at each injection step, a personalized linear model is identified by means of the linear least-squares method.
5) *Fault Detection:* the personalized linear model parameters are compared with the tolerance range calculated after the preliminary off-line metrological characterization of the device.
6) *Bioavailability Monitoring:* insulin bioavailability is calculated by assessing the insulin disappearance from the volume of investigated tissue.

III. Realization

In this section, prototyping of the hardware, the firmware, and the software is presented.

A. Hardware

The bioimpedance transducer was realized by exploiting off-the-shelf components. In particular, the EVAL-AD5940BIOZ of analog devices was used to implement the impedance meter block. The EVAL-AD5940BIOZ is composed of two boards, as shown in Fig. 2.

The down-board hosts the ADuCM 3029 chip provided with an ultralow power Arm Cortex-M3 MCU, 256 kB of embedded flash memory, and a 12-bit SAR ADC with a sampling rate of 1.8 MSa/s.

Moreover, the down-board has two wireless connectivity options (i.e., Bluetooth Low Energy 5.0 and Wifi Module) and connectors used for setting the on-board MCUs.

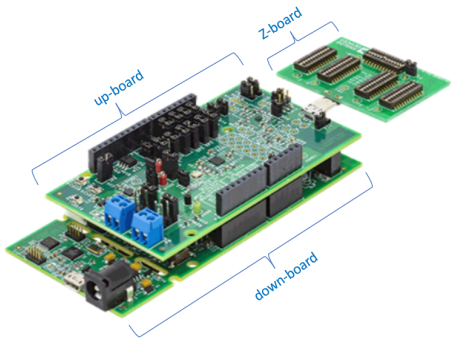

Fig. 2. Eval-AD5940BIOZ board.

The up-board hosts two high-precision excitation loops based on a 12-bit DAC with 200 kSa/s and a 16-bit ADC with both 800 kSa/s and 1.6 MSa/s options. The low-power excitation loop produces signals from dc to 200 Hz; while the high-power excitation produces signals up to 200 kHz. Moreover, the up-board operates a DFT up to 16 384 points computing both the real and imaginary parts of the impedance. The AD5940BIOZ is equipped with a Z test board, which models body impedance and electrode contact impedance.

B. Firmware and Software

The firmware for the impedance meter block was realized on the basis of libraries provided by Analog Device [37]. The firmware prototyping aimed to maximize the measurement throughput without penalizing the metrological characteristics of the transducer. In particular: 1) firmware architecture was articulated in ten different treads to take advantage of parallelization and 2) data transmission was scheduled only at the end of an entire measurement cycle. The device can be used in stand-alone mode (battery) or in connection with PC via COM port.

An interface was propotyped in C# to allow the following inputs and outputs.

1) *Data Acquisition Mode*: 1) fixed number of data to acquire and 2) continuous data acquisition.
2) Stimulus amplitude.
3) *Stimulus Frequency*: 1) fixed frequency and 2) frequency sweep in a chosen band.
4) Graphical and tabular data representation in the time and frequency domains.

Moreover, the data can be exported as CSV file for successive analysis.

IV. Laboratory and In Vitro Metrological Characterization

Metrological characterization in the laboratory focuses on the impedance meter block through the use of passive electrical components. Then, the human tissues are emulated by eggplants, and a preliminary characterization of the bioimpedance transducer is performed. Moreover, the compatibility of the electrical behavior of two substances (with and without insulin) is evaluated in view of subsequent in vivo characterization.

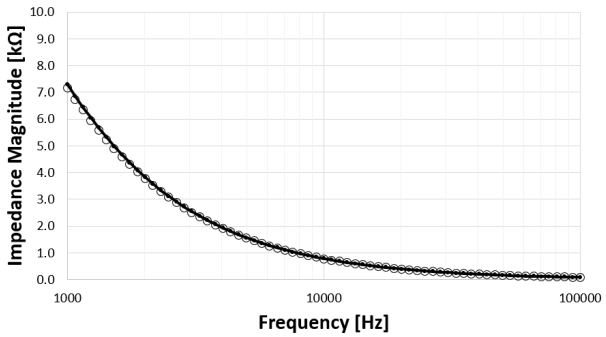

Fig. 3. Comparison between reference and measured impedance magnitude.

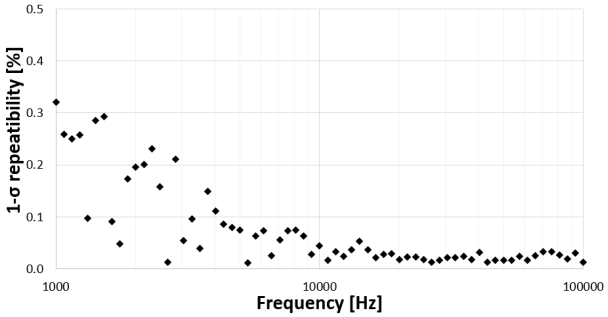

Fig. 4. Impedance magnitude percentage 1-σ repeatability.

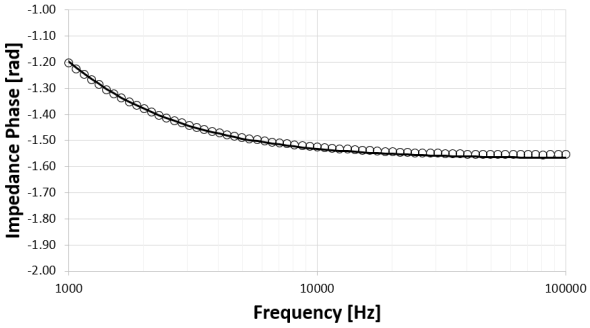

Fig. 5. Comparison between reference and measured impedance phase.

A. Laboratory

A parallel of a capacitor and a resistor was used to approximate the typical impedance behavior of human tissue. The equivalent electrical circuit was obtained using General Radio standard capacitor (0.02 μF) type 509-F and Uniohm 85 005 decade resistor (20 000 Ω). Ten cycles of measurements were realized at 100 frequencies equispaced from 100 Hz to 100 kHz on a logarithmic scale. The applied voltage amplitude was 100 mV. The mean and standard deviation of impedance magnitude were computed. In Figs. 3 and 4, the results are compared with the theoretical values after deterministic error compensation.

The σ repeatability is the variance associated with repeatability. It is a nonnegative parameter characterizing the dispersion of the quantity values being attributed to a measurand when out of a set of conditions are guaranteed: 1) the same measurement procedure; 2) same operators; 3) same measuring system; 4) same operating conditions and same location; and 5) replicate measurements on the same or similar objects over a short period of time.

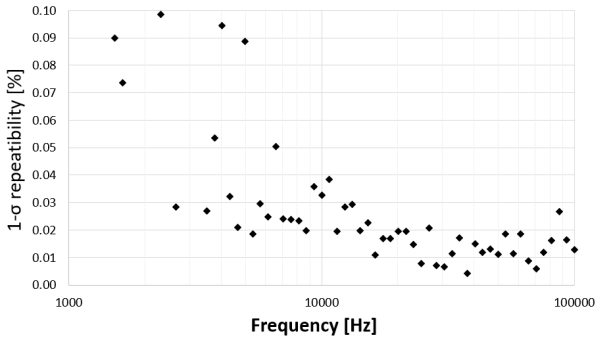

Fig. 6. Impedance phase percentage 1-σ repeatability.

The percentage 1-σ repeatability for each applied frequency is shown in Figs. 5 and 6 for magnitude and phase, respectively. For each frequency, it was calculated as the percentage of the mean standard deviation with respect to the mean.

As far as impedance magnitude is concerned, the highest value is 0.35%, while 0.10% was not exceeded, above 4 kHz. As far as impedance phase is concerned, the highest value is 0.1%, while 0.05% was not exceeded, above 8 kHz.

In the bandwidth of interest, typical percentage deterministic errors of 1% for both magnitude and phase were obtained. The mean 1-σ repeatability of impedance magnitude and phase were 1.8 Ω and 0.0005 rad, respectively.

B. In Vitro

The in vitro metrological characterization was realized on eggplants for their effectiveness of emulating human electrical behavior [38]. Moreover, a negligible dielectric dispersion can be considered in the frequency bandwidth interested for both the tissues [39], [40]. As a matter of fact, eggplants introduced some limitations in the analysis. Indeed, the human tissue is subject to more mechanical noise sources than eggplants (such as breathing). Moreover, the human tissue exhibits a more complex and rapid time variation with respect to eggplants. However, it is important to emphasize the measurement phase when the emulation of human tissue through eggplant is used, namely, the appearance phase. In this phase, a quasi-static approximation of human tissue metabolic behavior is assumed by adopting a measurement time under 2 min. Indeed, during this period only 2% of a typical insulin bolus is on average absorbed [41].

In particular, the experimental campaign was realized by means of two different substances, namely, an insulin-based solution and its solvent (vehicle) both produced by Lilly [42].

Therefore, reproducibility, repeatability, sensitivity, uncertainty, accuracy, and nonlinearity were assessed by varying the injected substance.

Twenty eggplants were peeled and dried at 23 °C for two hours. Subsequently, they were cut in samples of 10 cm × 4 cm × 4 cm. Four FIAB PG500 electrodes of 14 mm × 36 mm were placed on the eggplants evenly spaced by 5 mm. A sinusoidal voltage amplitude of 100 mV was applied on the eggplants at a frequency of 1 kHz. The frequency was chosen to maximize the sensitivity as highlighted in [36]. The injections were administered by exploiting a Lilly's 100 U/ml Insulin Pen and Lilly's Saline Kiwin Pen with a needle of length 4 mm. The Insulin Pen contains an insulin dissolved in a vehicle solution, and the Saline Kiwin Pen contains only the vehicle composed of m-cresol, glycerol, dibasic sodium phosphate 7H2O, and zinc oxide dissolved in sterile water for injectable preparations.

The eggplant impedance was assessed after five consecutive substance injections of 20 μl (2 IU). At the end of each injection (*measurement point*), ten consecutive measurements were acquired and their average value (*impedance score*) was computed. The mean impedance value after needle introduction (reference) was used for subsequent comparisons. Ten eggplants were selected for insulin administrations and ten for vehicle administrations.

A PIV was calculated between the impedance score of each measurement point and the reference. For each eggplant, a was calculated as the regression line (least-squares algorithm) in the plane of PIV and the amount of substance injected. The mean of the PIV (MPIV) of the eggplant samples for each amount of insulin injected was computed. The *generic model* is the regression line calculated in the plane of MPIV and the amount of vehicle injected.

1) Reproducibility: For each measurement point, the standard deviation of the ten eggplant PIV was calculated. Finally, the percentage 1-σ reproducibility was calculated as the percentage of the mean standard deviation with respect to the overall mean of the PIVs.

As concerns the insulin injections, a 1-σ reproducibility of 71% and 89% for magnitude and phase was assessed, respectively. As concerns the vehicle injections, a 1-σ reproducibility of 74% and 58% for magnitude and phase was obtained, respectively. The decrease in the reproducibility of phase measurements is linked to different compositions of two substances. In particular, insulin is composed of macromolecules which increase the impact of heterogeneity of the eggplant porosity on the electrical behavior of the substance.

2) Repeatability: Ten consecutive measurements were acquired for each measurement point and ordered into a vector [one vector for needle introduction (v_1) and five for five consecutive injections ($v_{i1}, v_{i2}, \ldots, v_{i5}$)]. Each value in v_i vectors was overwritten with its PIV with respect to the correspondent value in (v_1). Finally, the 1-σ repeatability was obtained as the mean of the standard deviation of each vector v_i.

Regarding insulin injections, mean values of 0.45% and 1.9% were obtained for impedance magnitude and phase, respectively. As concerns vehicle injections, mean values of 0.79% and 3.11% were assessed for impedance magnitude and phase, respectively.

3) Sensitivity: The sensitivity was calculated by the slope of the linear model both in case of generic and personalized models. A comparison between the generic models obtained after vehicle and insulin administrations is reported in Figs. 7 and 8, respectively.

The two trends appeared compatible, namely, increasing the substance amount, the impedance magnitude monotonously decreases and the impedance phase monotonously increases, both within the same order of magnitude.

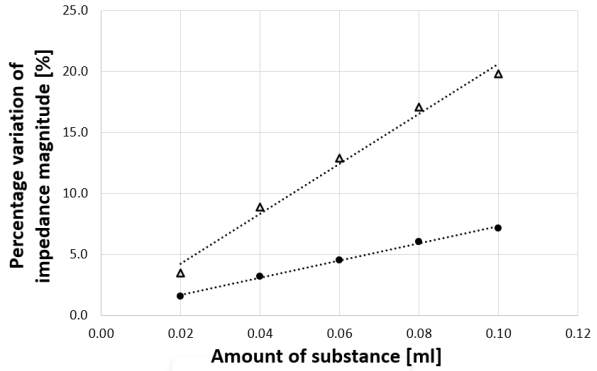

Fig. 7. Mean percentage impedance magnitude variation versus amount of vehicle (triangles) and insulin (points) injected, in in vitro tests.

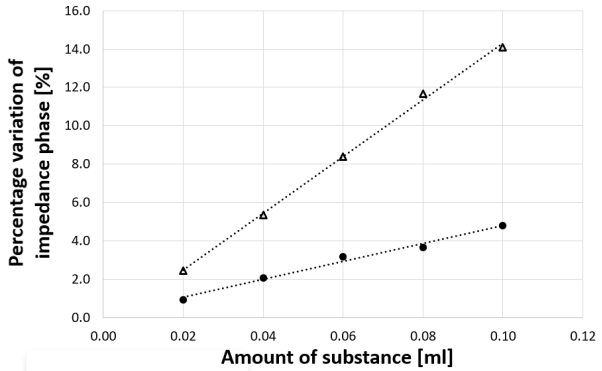

Fig. 8. Mean percentage impedance phase variation versus amount of vehicle (triangles) and insulin (points) injected, in in vitro tests.

TABLE I

CONDUCTIVITY OF DISTILLED WATER WITH 1 PPM IMPURITY CONCENTRATION, INSULIN, AND VEHICLE AT 10 KHZ

substance	conductivity [mS/m]
distilled water (1 ppm)	0.20
insulin	3.20
vehicle	15.20

As far as the insulin generic model is concerned, the mean sensitivity values of 69.98 and 48.83 ml^{-1} were obtained for impedance magnitude and phase, respectively. As regards the vehicle generic model, the mean sensitivity values of 204.77 and 148.03 ml^{-1} were obtained for impedance magnitude and phase, respectively.

Figs. 7 and 8 highlight the compatibility between the electrical behavior of the substances. Indeed, for both the substances a direct linear relationship between substance amount and impedance variation can be identified. However, the transducer showed greater sensitivity to vehicle than insulin due to different conductivities (although compatible if compared with the conductivity of distilled water) of the two investigated substances, as reported in Table I.

Regarding the personalized models, the sensitivity values obtained are reported in Table II.

4) Nonlinearity: The nonlinearity was calculated by means of the residual standard deviation

$$\sqrt{\frac{\sum_{i=1}^{n}(y_i - \widehat{y}_i)^2}{n-2}} \tag{1}$$

TABLE II

BIOIMPEDANCE TRANSDUCER SENSITIVITY IN IN VITRO TESTS

Sample	*Insulin* Magnitude ml^{-1}	*Insulin* Phase ml^{-1}	Sample	*Vehicle* Magnitude ml^{-1}	*Vehicle* Phase ml^{-1}
1	100.07	69.95	11	76.31	102.92
2	29.01	5.86	12	465.62	102.92
3	119.79	79.75	13	169.52	165.61
4	115.86	68.31	14	363.93	303.54
5	20.65	24.12	15	116.24	84.76
6	63.31	48.85	16	296.8	160.36
7	14.22	51.02	17	77.42	120.21
8	20.53	13.50	18	128.95	101.99
9	165.87	85.64	19	312.95	168.26
10	50.49	21.33	20	39.95	14.13
Mean	69.98	46.83		204.77	160.07
Std Dev	52.47	28.99		137.21	101.88
Generic Model	69.98	48.83		204.77	148.03

TABLE III

BIOIMPEDANCE TRANSDUCER PERCENTAGE NONLINEARITY IN IN VITRO TESTS

Sample	*Insulin* Magnitude %	*Insulin* Phase %	Sample	*Vehicle* Magnitude %	*Vehicle* Phase %
1	1.93	3.73	11	16.95	15.47
2	21.69	50.89	12	2.36	6.98
3	3.06	7.52	13	4.40	14.06
4	4.00	52.61	14	8.28	14.14
5	6.44	10.21	15	7.48	9.07
6	16.03	15.88	16	5.84	10.06
7	9.32	18.03	17	5.49	18.57
8	13.95	16.63	18	5.68	13.08
9	11.36	63.81	19	18.56	10.65
10	0.43	0.96	20	9.44	19.53
Mean	9.03	24.20		8.45	5.31
Std Dev	6.65	22.63		13.16	4.05
Generic Model	2.45	5.18		5.05	2.58

where

1) n is the number of injection steps;
2) y is the experimental value of the percentage variation; and
3) $\widehat{y}$ is the percentage variation value calculated through the equation of regression line.

Then, the percentage of nonlinearity was calculated with respect to the range of variation in y.

As far as the insulin injections, nonlinearity values of 2.45% and 5.18% for impedance magnitude and phase were assessed, respectively, for the generic model. As concerns the vehicle injections, nonlinearity values of 5.05% and 2.58% for impedance magnitude and phase were assessed, respectively, for the generic model. Regarding the personalized models, the results are shown in Table III.

5) Accuracy: The rms of the deterministic error (RMSE) for the generic model and the average RMSE among the personalized models, as the amount of vehicles and insulin varies, are compared in Figs. 9 and 10 for impedance magnitude and phase, respectively.

For both the substances, the personalized models exhibit a lower accuracy with respect to the generic models.

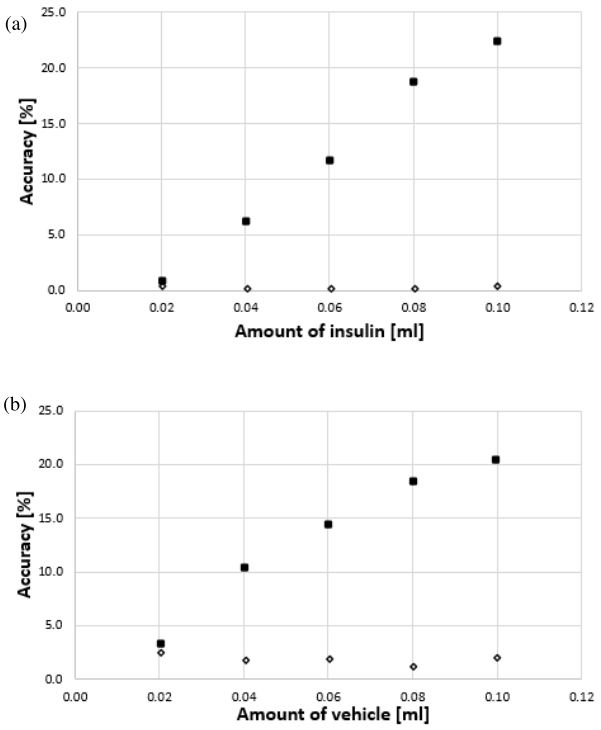

Fig. 9. (a) Impedance magnitude percentage accuracy of personalized (rumbles) and generic (squares) model versus amount of insulin for impedance phase, in vitro experiments. (b) Impedance magnitude percentage accuracy of personalized (rumbles) and generic (squares) model versus amount of vehicle, in in vitro experiments.

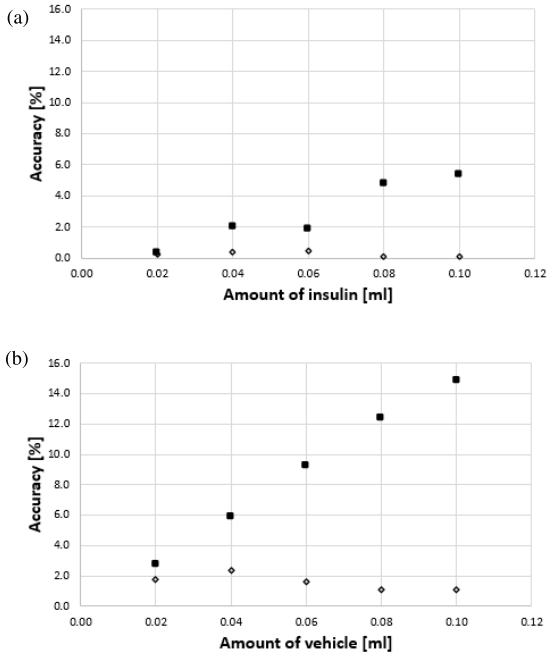

Fig. 10. (a) Impedance phase percentage accuracy of personalized (rumbles) and generic (squares) model versus amount of insulin for impedance phase, in vitro experiments. (b) Impedance phase percentage accuracy of personalized (rumbles) and generic (squares) model versus amount of vehicle, in in vitro experiments.

As impedance magnitude is concerned, the substances showed accuracy below 5.0%.

The results showed higher sensitivity and nonlinearity of the vehicle with respect to the insulin. However, the same monotonic relationship between impedance variation and amount of substance injected was observed. Moreover, for both the substances, the generic model exhibits a lower nonlinearity and a higher accuracy with respect to the mean nonlinearity and accuracy of the personalized models.

Fig. 11. Subject's abdomen during vehicle injection cycle.

V. In Vivo Metrological Characterization

A. Experimental Setup

As explained in Section IV-B, eggplants well emulate human electrical behavior. Moreover, the results of in vitro metrological characterization showed the compatibility of the electrical behavior of insulin and vehicle. In general, the patient with diabetes injects a variable bolus dose (depending on the subjective conditions and type of meal). Therefore, the experiments were realized on a healthy subject by only injecting vehicle, to improve the experimental reproducibility.

The volunteer signed the informed consent prior to the tests, and all the procedures were carried out in compliance with the appropriate guidelines. The Ethical Review Committee (number 238/18) of the University of Naples Federico II approved the research. All the electronic devices were removed from the measurement zone. The experiments were conducted in a controlled temperature room. Over the course of a month, the volunteer was subject to 12 injection cycle of 100 μl of vehicle. In particular, five consecutive injections of 20 μl were performed for each injection cycle. The measurements were realized by setting a sinusoidal voltage amplitude of 100 mV at a frequency of 10 kHz. The frequency was chosen to relax the safety requirement for peak current (IEC-60601 standard) and to minimize the impact of physiological phenomena (e.g. muscle contraction and blood flow) more relevant at lower frequencies.

The bioimpedance transducer was connected to a laptop set to battery power mode. The laptop's screen showed simultaneously: 1) the impedance value trend and 2) the subject abdomen recorded with laptop's internal camera to observe that all the setup conditions were respected during the experiment. All the cycles of the experimental campaign were video-recorded to allow ex post verification on the parameters of the experimental setup (e.g. electrodes' adhesion) using zoom and slowmotion.

As reported in Fig. 11, the subject was asked to maintain an upright position during the acquisitions as this condition had improved repeatability in preliminary experiments.

Four FIAB 500 electrodes of 14 mm $\times$ 36 mm were positioned on the abdomen with an interelectrodic distance of 1 cm. Lilly's Saline Kiwin Pen with a needle of length 4 mm was used for injection. Vehicle administration was performed

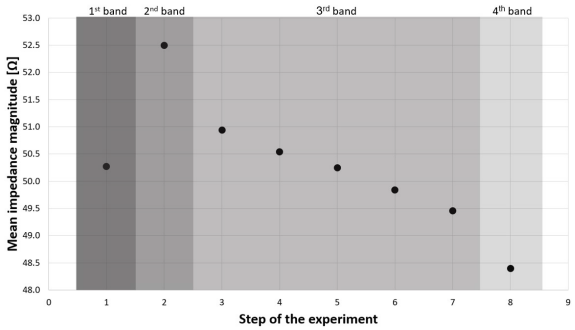

Fig. 12. Mean impedance magnitude trend of the eight experimental steps in in vivo tests. The first and second bands highlight the baseline and needle introduction steps, respectively. The third band groups the five steps of vehicle administration. The needle extraction step is marked by the fourth band.

by placing the pen between the voltmetric electrodes and keeping it perpendicularly to the surface of the abdominal tissue.

The experimental campaign was characterized by eight steps (Fig. 12). The first step is the preinjecting condition (baseline), while the second step occurs with needle insertion (reference). The third to seventh steps are the five successive administrations of 20 μl of vehicle and, finally, the eighth step occurs with needle extraction. The mean time between injections and bioimpedance measurements is 5 s, waiting for the mechanical transient attenuation. In this way, the total duration of a measurement cycle remains below 2 min.

B. Results

Differently from the laboratory and in vitro experiments, only the impedance magnitude results are reported owing to the non-monotonicity of the phase at varying the amount of substance.

As shown in Fig. 12, needle introduction produced a considerable increase in the impedance magnitude because of the pressure exerted on the abdomen to hold the syringe in place. Therefore, the impedance score after needle introduction (reference) is used for subsequent comparisons. A PIV was calculated between the impedance score of each step and the reference. For each measurement cycle, a personalized model was identified as the regression line (least-squares algorithm) in the plane of PIV and amount of vehicle injected.

Then, the MPIV among the 12 measurement cycles for each amount of insulin injected was computed. The *generic model* is the regression line calculated in the plane of MPIV and the amount of vehicle injected.

1) Reproducibility: For each measurement point, the standard deviation of the PIV among the 12 cycles was calculated. Finally, the percentage 1-σ reproducibility was calculated as the percentage of the mean standard deviation with respect to the overall mean of the PIVs. A 1-σ intercycles' reproducibility of 36% was assessed. A comparison between the reproducibility of the present study and the state-of-the-art is reported in Table IV.

2) Repeatability: Ten consecutive measurements were acquired for each measurement point and ordered into a vector [one vector for needle introduction (v_1) and five for the five consecutive injections ($v_{i1}, v_{i2}, \ldots, v_{i5}$)]. Each value in v_i vectors was overwritten with its PIV with respect to the correspondent value in (v_1). Finally, the 1-σ repeatability was obtained as the mean of the standard deviation of each vector v_i.

A 1-σ repeatability of 0.35% was obtained.

3) Sensitivity: A sensitivity of 33.76 ml^{-1} was obtained for the generic model. The sensitivity was the slope of the model in the plane of PIV and the amount of substance [Fig. 13(a)]. Regarding the personalized models, the sensitivity values are reported in Table V.

TABLE IV
COMPARISON BETWEEN THE REPRODUCIBILITY OF THE PRESENT STUDY AND THE PREVIOUS ONE

Article	Reproducibility [%]
[30]	285
present study	36

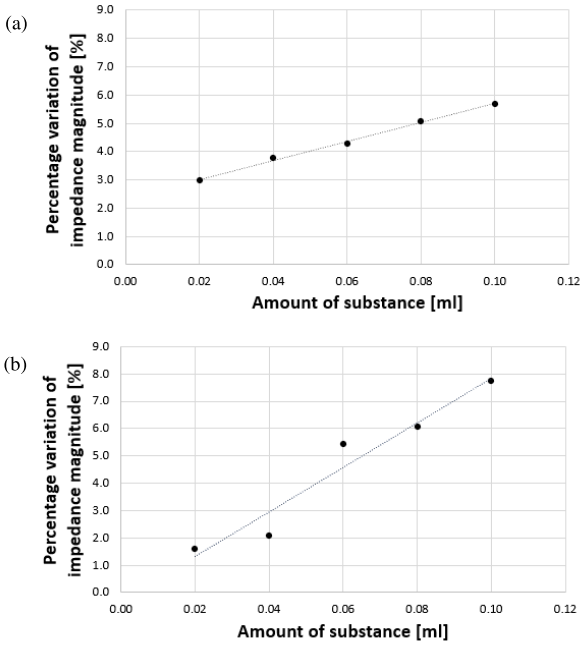

Fig. 13. Percentage impedance magnitude variation versus amount of vehicle injected in in vivo experiments. (a) Generic model. (b) Personalized model obtained from 11th cycle.

TABLE V
BIOIMPEDANCE TRANSDUCER SENSITIVITY AND NONLINEARITY IN IN VIVO TESTS

Cycle	*Sensitivity*	*Non-linearity*
	ml^{-1}	%
1	69.16	7.31
2	31.19	30.65
3	63.64	11.93
4	16.21	20.62
5	28.39	11.63
6	21.65	28.06
7	13.28	13.45
8	37.41	12.41
9	81.43	11.82
10	6.26	6.79
Mean	36.86	14.47
Std Dev	25.82	7.07
Generic Model	33.76	2.76

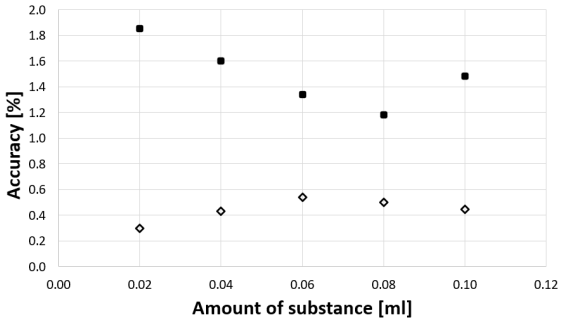

Fig. 14. Accuracy of personalized (rumbles) and generic (squares) model versus amount of vehicle, in in vivo experiments.

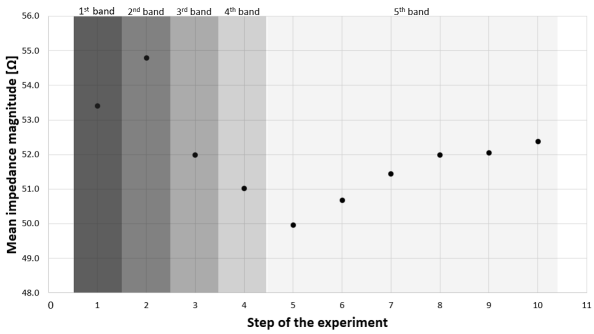

Fig. 15. Mean impedance magnitude trend of the ten experimental steps in absorption test on a human volunteer. The first and second bands highlight the baseline and the needle introduction steps, respectively. The third band corresponds to vehicle administration. The needle extraction step is marked by the fourth band. The fifth band groups the steps during the disappearance of the vehicle from the site of injection.

4) Nonlinearity: The percentage nonlinearity was 2.76% for the generic model. As concerns the personalized models, the results are shown in Table V. As shown in Fig. 13, the generic model exhibits a lower linearity than the personalized models.

5) Accuracy: The rms of the deterministic error (RMSE) for the generic model and the average RMSE among the personalized models as the amount of vehicles varies are compared in Fig. 14.

As shown in Figs. 13 and 14, the personalized models guarantee a lower accuracy with respect to the generic model but exhibit higher nonlinearity. Moreover, the personalized models showed an accuracy comparable to the accuracy obtained in the in vitro tests even though the human tissue is subject to mechanical noise sources and has time-varying composition.

In clinical applications, the inverse model (disappearance model) has to be used to assess the drug absorbed from the measured impedance variation. In this framework, an accuracy related to the vehicle amount assessment can be computed from the accuracy of the direct model (appearance model). In particular, the *accuracy for clinical applications* is computed as the ratio between the accuracy and the sensitivity of the direct model. Therefore, it is possible to estimate an accuracy for clinical application of 12 μl, given the average sensitivity of 36.86 ml^{-1}.

In [33], different models of the relationship between the percentage impedance magnitude variation and the amount of substance administered were compared. The second-order polynomial model improved the metrological performance of the bioimpedance transducer with respect to the linear model. The accuracy of the direct model was improved by 37% by applying a second-order model on the data acquired during in vivo experimental campaign. The average sensitivity computed among the ten nonlinear personalized models was 31.00 ml^{-1}. Therefore, the accuracy for clinical application, when a second-order model is adopted, improved to 9 μl.

6) Uncertainty: Two main sources of uncertainty were considered: 1) the instrument and 2) the measurand. Instrumental uncertainty (u_i) was calculated as the ratio between σ_u and the square root of 10 (the number of repeated measurements), where σ_u is the product between percentage 1-σ repeatability at 10 kHz obtained from laboratory tests and Δy, namely, the typical range of PIV during in vivo experiments. The measurand uncertainty (u_m) was calculated as the ratio between the mean 1-σ repeatability from in vivo tests and the square root of 10. The combined uncertainty (u_c) of the direct model was calculated as the root sum squared of (u_i and u_m).

An *uncertainty for clinical applications* of 4.2 μl was computed as the ratio between u_c and the mean sensitivity of personalized models.

C. Discussion

As the impedance phase is concerned, non-monotonicity was observed in contrast to laboratory and in vitro results. The relative complex effective dielectric permittivity of tissues is modified by the introduction of substances. The impact of these changes on the impedance phase requires the use of more complex models yet to be identified.

As the impedance magnitude is concerned, a large decrease in percentage 1-σ intraindividual reproducibility was reported with respect to the state-of-the-art (from more than 200% to 36%). This result confirms the containment of the mechanical uncertainty sources. In particular, the subdivision of the measurement in eight steps allowed the identification of three fundamental events: baseline, needle insertion, and needle extraction. Typically, needle insertion and extraction determines impedance variations in comparable amplitude and opposite sign, due to the mechanical stress to which the tissue is subjected [33]. The bioimpedance transducer builds the personalized model by adopting as initial impedance value the measurement acquired after the insertion of needle. Then, the personalized model is identified before needle extraction. This way, a first stage of filtering the mechanical source of uncertainly is implemented. Subsequently, the mechanical transient attenuation checker operates during the whole measure to filter the remaining mechanical effects due to substance administration.

VI. Absorption Assessment Feasibility

An exploratory test was conducted on the healthy subject to assess the impedance variation due to vehicle absorption. The volunteer was subjected to a single injection of 100 μl of vehicle.

The test was characterized by ten steps. The first step is the preinjecting condition, the second step arises from needle insertion, the third step represents the administration of 100 μl of vehicle, and the fourth step occurs with needle extraction.

Finally, the absorption phase groups the steps from number five to ten. The first five steps last 20 s, while in the absorption phase each step lasts 10 min. Steps are characterized by their impedance scores.

As shown in Fig. 15, impedance magnitude decreases during the first five steps. From the sixth to the tenth step, a tendency for impedance magnitude to return to the pre-injection condition was observed. The impedance decrease during the fifth step could be related to the diffusion of the vehicle within the tissue under investigation before passing into the bloodstream. After the fifth step, the impedance increase reflects the disappearance of the substance from the injection site, namely, vehicle absorption.

VII. Conclusion

A low-cost bioimpedance transducer for noninvasive and real-time monitoring of insulin bioavailability after subcutaneous injection was prototyped and metrologically characterized. Combining low-cost, noninvasiveness, and low latency represents a novelty in the insulin bioavailability assessment field. The limitations of the study concern: 1) the lack of model able to explain the nonmonotonic trend in the relationship between the impedance phase variation and the amount of vehicle injected and 2) the number of subjects enrolled in the study, namely, one (even if 12 injection cycles were performed).

As the impedance phase is concerned, typical percentage deterministic errors of 1% and mean 1-σ repeatability 0.05% radiant were obtained in the bandwidth of interest during the laboratory tests. Good trends of monotonicity and linearity emerged during in vitro tests.

As the impedance magnitude is concerned, the results of the in vitro metrological characterization showed the compatibility of the electrical behavior of insulin and vehicle. In general, the patient with diabetes injects a variable bolus dose (depending on the subjective conditions and type of meal). Therefore, the experiments were realized on a healthy subject by only injecting vehicle, to improve the experimental reproducibility.

During in vivo tests, a large decrease in percentage 1-σ intraindividual reproducibility was reported with respect to the state-of-the-art (from more than 200% to 36%). This result can be related to the containment of the mechanical uncertainty sources. An accuracy for clinical applications of 9 μl was obtained by means of a second-order polynomial model. Uncertainty for clinical applications resulted well below the typical volume of one insulin unit (10.0 μl), namely, 4.2 μl.

Future works will be focused on: 1) identification of the relationship between impedance phase variation and drug amount in case of human tissue; 2) verification of the in vivo results by improving the experimental sample size; 3) finite element modeling of human tissue injected with drug for improving the uncertainty sources' analysis; and 4) an experimental campaign on patients with diabetes to clinically validate the bioimpedance transducer.

Acknowledgment

The authors thank the editor and the anonymous reviewers for their stimulating and precious suggestions and comments to the review of this article. The authors thank Giusy Carleo for performing measurements on eggplants.

References

[1] D. Atlas et al., "International diabetes federation," in *IDF Diabetes Atlas*, 7th ed. Brussels, Belgium: Int. Diabetes Fed., vol. 33, 2015, p. 2.

[2] J. A. Bluestone, K. Herold, and G. Eisenbarth, "Genetics, pathogenesis and clinical interventions in type 1 diabetes," *Nature*, vol. 464, no. 7293, pp. 1293–1300, Apr. 2010.

[3] J. A. Todd, "Etiology of type 1 diabetes," *Immunity*, vol. 32, no. 4, pp. 457–467, 2010.

[4] M. A. Atkinson, G. S. Eisenbarth, and A. W. Michels, "Type 1 diabetes," *Lancet*, vol. 383, no. 9911, pp. 69–82, 2014.

[5] T. Karacolak, A. Z. Hood, and E. Topsakal, "Design of a dual-band implantable antenna and development of skin mimicking gels for continuous glucose monitoring," *IEEE Trans. Microw. Theory Techn.*, vol. 56, no. 4, pp. 1001–1008, Apr. 2008.

[6] I. B. Hirsch, "Realistic expectations and practical use of continuous glucose monitoring for the endocrinologist," *J. Clin. Endocrinol. Metabolism*, vol. 94, no. 7, pp. 2232–2238, Jul. 2009.

[7] J. Yadav, A. Rani, V. Singh, and B. M. Murari, "Prospects and limitations of non-invasive blood glucose monitoring using near-infrared spectroscopy," *Biomed. Signal Process. Control*, vol. 18, pp. 214–227, Apr. 2015.

[8] N. Spegazzini et al., "Spectroscopic approach for dynamic bioanalyte tracking with minimal concentration information," *Sci. Rep.*, vol. 4, no. 1, pp. 1–7, Nov. 2014.

[9] W. Villena Gonzales, A. Mobashsher, and A. Abbosh, "The progress of glucose monitoring—A review of invasive to minimally and non-invasive techniques, devices and sensors," *Sensors*, vol. 19, no. 4, p. 800, Feb. 2019.

[10] N.-Y. Kim, K. K. Adhikari, R. Dhakal, Z. Chuluunbaatar, C. Wang, and E.-S. Kim, "Rapid, sensitive and reusable detection of glucose by a robust radiofrequency integrated passive device biosensor chip," *Sci. Rep.*, vol. 5, no. 1, pp. 1–9, Jan. 2015.

[11] M. Baghelani, Z. Abbasi, M. Daneshmand, and P. E. Light, "Non-invasive continuous-time glucose monitoring system using a chipless printable sensor based on split ring microwave resonators," *Sci. Rep.*, vol. 10, no. 1, pp. 1–15, Jul. 2020.

[12] K. K. Adhikari and N.-Y. Kim, "Ultrahigh-sensitivity mediator-free biosensor based on a microfabricated microwave resonator for the detection of micromolar glucose concentrations," *IEEE Trans. Microw. Theory Techn.*, vol. 64, no. 1, pp. 319–327, Jan. 2016.

[13] V. Katseli, A. Economou, and C. Kokkinos, "Smartphone-addressable 3D-printed electrochemical ring for nonenzymatic self-monitoring of glucose in human sweat," *Anal. Chem.*, vol. 93, no. 7, pp. 3331–3336, Feb. 2021.

[14] C. Cobelli, E. Renard, and B. P. Kovatchev, "Artificial pancreas: Past, present, future," *Diabetes*, vol. 60, no. 1, pp. 2672–2682, 2011.

[15] A. Basu et al., "Time lag of glucose from intravascular to interstitial compartment in humans," *Diabetes*, vol. 62, pp. 4083–4087, Dec. 2013.

[16] R. J. Young, W. J. Hannan, B. M. Frier, J. M. Steel, and L. J. P. Duncan, "Diabetic lipohypertrophy delays insulin absorption," *Diabetes Care*, vol. 7, no. 5, pp. 479–480, Sep. 1984.

[17] K. Mandava, S. Cherukuri, U. Batchu, V. Cherukuri, and K. Ganapuram, "Formulation and evaluation of transdermal drug delivery of topiramate," *Int. J. Pharmaceutical Invest.*, vol. 7, no. 1, p. 10, 2017.

[18] S. F. Cordery et al., "Topical bioavailability of diclofenac from locally-acting, dermatological formulations," *Int. J. Pharmaceutics*, vol. 529, nos. 1–2, pp. 55–64, Aug. 2017.

[19] S. Eirefelt et al., "Evaluating dermal pharmacokinetics and pharmacodynamic effect of soft topical PDE4 inhibitors: Open flow microperfusion and skin biopsies," *Pharmaceutical Res.*, vol. 37, no. 12, pp. 1–12, Dec. 2020.

[20] L. Ayalew et al., "C-terminal lysine processing of IgG in human suction blister fluid: Implications for subcutaneous administration," *Mol. Pharmaceutics*, vol. 19, no. 11, pp. 4043–4054, Nov. 2022.

[21] B. A. Kuzma, S. Senemar, T. Ramezanli, P. Ghosh, S. G. Raney, and G. Stagni, "Evaluation of local bioavailability of metronidazole from topical formulations using dermal microdialysis: Preliminary study in a Yucatan mini-pig model," *Eur. J. Pharmaceutical Sci.*, vol. 159, Apr. 2021, Art. no. 105741.

[22] S. Y. Chaw, T. T. L. Wong, S. Venkatraman, and A.-M. Chacko, "Spatio-temporal in vivo imaging of ocular drug delivery systems using fiberoptic confocal laser microendoscopy," *J. Visualized Exp.*, vol. 175, Jan. 2021, Art. no. e62685.

[23] M. N. Afsar, A. Moonshiram, and Y. Wang, "Assessment of random and systematic errors in millimeter-wave dielectric measurement using open resonator and Fourier transform spectroscopy systems," *IEEE Trans. Instrum. Meas.*, vol. 53, no. 4, pp. 899–906, Aug. 2004.

[24] U. A. Khan, N. Nguyen, and M. N. Afsar, "Millimeter- and submillimeter-wave dielectric measurements of household powders using Fourier transform spectroscopy," *IEEE Trans. Instrum. Meas.*, vol. 57, no. 2, pp. 286–293, Feb. 2008.

[25] D. Das, F. A. Kamil, S. Agrawal, K. Biswas, and S. Das, "Fragmental frequency analysis method to estimate electrical cell parameters from bioimpedance study," *IEEE Trans. Instrum. Meas.*, vol. 63, no. 8, pp. 1991–2000, Aug. 2014.

[26] D. Chowdhury and M. Chattopadhyay, "Study and classification of cell bio-impedance signature for identification of malignancy using artificial neural network," *IEEE Trans. Instrum. Meas.*, vol. 70, pp. 1–8, 2021.

[27] R. Baghbani, M. B. Shadmehr, M. Ashoorirad, S. F. Molaeezadeh, and M. H. Moradi, "Bioimpedance spectroscopy measurement and classification of lung tissue to identify pulmonary nodules," *IEEE Trans. Instrum. Meas.*, vol. 70, pp. 1–7, 2021.

[28] P. Arpaia, U. Cesaro, and N. Moccaldi, "Measuring the drug absorbed by biological tissues in laboratory emulation of dermatological topical treatments," in *Proc. IEEE Int. Symp. Med. Meas. Appl. (MeMeA)*, May 2016, pp. 1–5.

[29] P. Arpaia, U. Cesaro, and N. Moccaldi, "A bioimpedance meter to measure drug in transdermal delivery," *IEEE Trans. Instrum. Meas.*, vol. 67, no. 10, pp. 2324–2331, Oct. 2018.

[30] P. Arpaia, U. Cesaro, M. Frosolone, N. Moccaldi, and M. Taglialatela, "A micro-bioimpedance meter for monitoring insulin bioavailability in personalized diabetes therapy," *Sci. Rep.*, vol. 10, no. 1, pp. 1–11, Aug. 2020.

[31] S. M. Moqadam, P. Grewal, M. Shokoufi, and F. Golnaraghi, "Compression-dependency of soft tissue bioimpedance for in-vivo and in-vitro tissue testing," *J. Electr. Bioimpedance*, vol. 6, no. 1, pp. 22–32, Dec. 2015.

[32] R. Kusche and M. Ryschka, "Respiration monitoring by combining EMG and bioimpedance measurements," in *Proc. World Congr. Med. Phys. Biomed. Eng.* Cham, Switzerland: Springer, 2019, pp. 847–850.

[33] P. Arpaia, D. Cuneo, F. Mancino, S. Minucci, N. Moccaldi, and I. Sannino, "Preliminary investigation of the impact of mechanical stresses on bioimpedance spectroscopy-based insuline bioavailability assessment," in *Proc. Int. Workshop Impedance Spectrosc. (IWIS)*, Oct. 2021, pp. 52–55.

[34] J.-J. Cabrera-López and J. Velasco-Medina, "Structured approach and impedance spectroscopy microsystem for fractional-order electrical characterization of vegetable tissues," *IEEE Trans. Instrum. Meas.*, vol. 69, no. 2, pp. 469–478, Feb. 2020.

[35] C. Tan et al., "A wideband electrical impedance tomography system based on sensitive bioimpedance spectrum bandwidth," *IEEE Trans. Instrum. Meas.*, vol. 69, no. 1, pp. 144–154, Jan. 2020.

[36] P. Arpaia, U. Cesaro, and N. Moccaldi, "Noninvasive measurement of transdermal drug delivery by impedance spectroscopy," *Sci. Rep.*, vol. 7, no. 1, pp. 1–10, Mar. 2017.

[37] Analog Device. *Analog Device Libraries*. Accessed: Jan. 3, 2023. [Online]. Available: https://github.com/analogdevicesinc/ad5940-examples

[38] B. Rigaud, J.-P. Morucci, and N. Chauveau, "Bioelectrical impedance techniques in medicine Part I: Bioimpedance measurement second section: Impedance spectrometry," *Crit. Rev. Biomed. Eng.*, vol. 24, nos. 4–6, pp. 257–351, 1996.

[39] P. A. Hasgall et al., "IT'IS database for thermal and electromagnetic parameters of biological tissues," IT'IS Found., Zürich, Switzerland, Version 4.1, Feb. 2022. [Online]. Available: https://itis.swiss/database, doi: 10.13099/VIP21000-04-1.

[40] D. E. Khaled, N. N. Castellano, J. A. Gazquez, R. M. G. Salvador, and F. Manzano-Agugliaro, "Cleaner quality control system using bioimpedance methods: A review for fruits and vegetables," *J. Clean. Prod.*, vol. 140, pp. 1749–1762, Jan. 2017.

[41] C. Binder, T. Lauritzen, O. Faber, and S. Pramming, "Insulin pharmacokinetics," *Diabetes Care*, vol. 7, no. 2, pp. 188–199, 1984.

[42] Lilly. *Lilly Company Info*. Accessed: Jan. 3, 2023. [Online]. Available: https://www.lilly.it/

Pasquale Arpaia (Senior Member, IEEE) received the M.S. and Ph.D. degrees in electrical engineering from the University of Naples Federico II (UNINA), Naples, Italy, in 1987 and 1992, respectively.

He was an Associate Professor with the University of Sannio, Benevento, Italy. He is currently a Full Professor of instrumentation and measurements with UNINA and a Team Leader with CERN, Geneva, Switzerland. He is also the Head of the Interdepartmental Center for Research on Management and Innovation of Health (CIRMIS), the Head of the Hi-Tech Academic FabLab, Department of Electrical Engineering and Information Technology (DIETI), UNINA, and the Chairperson of the Stage Project of UNINA. He is also the Head of the Instrumentation and Measurement for Particle Accelerators Laboratory (IMPALab) and the Augmented Reality for Health Monitoring Laboratory (ARHeMlab). His current research interests include augmented reality, brain–computer interfaces, cyber-security, digital instrumentation and measurement techniques, evolutionary diagnostics, and distributed measurement systems.

Francesca Mancino received the M.S. degree (cum laude) in biomedical engineering from the University of Naples Federico II, Naples, Italy, in 2021, where she is currently pursuing the Ph.D. degree in information and communication technology for health.

She has authored or coauthored several scientific papers in journals and national and international conference proceedings in this field. Her current research interests include impedance spectroscopy-based method for drug bioavailability measurements in diabetology and orthopedics and electroencephalographic signal processing for executive function measurement.

Ms. Mancino won the IEEE Instrumentation and Measurement Graduate Fellowship Award 2021.

Nicola Moccaldi (Member, IEEE) received the M.A. degree in communication science from the University of Salerno, Fisciano, Italy, in 1999, and the M.Sc. degree in electronic engineering and the Ph.D. degree in information technologies and electrical engineering from the University of Naples Federico II (UNINA), Napoli, Italy, in 2018 and 2021, respectively.

He is currently the Scientific Coordinator of Passive BCI Research Line with the ARHeMLab of DIETI Excellence Department (Laboratory of Augmented Reality for Health Monitoring)—UNINA. His current research interests include biomedical instrumentation and measurement.

Dr. Moccaldi is a member of the IEEE Instrumentation and Measurement Society and the BCI Society.